Provided for non-commercial research and education use.
Not for reproduction, distribution or commercial use.

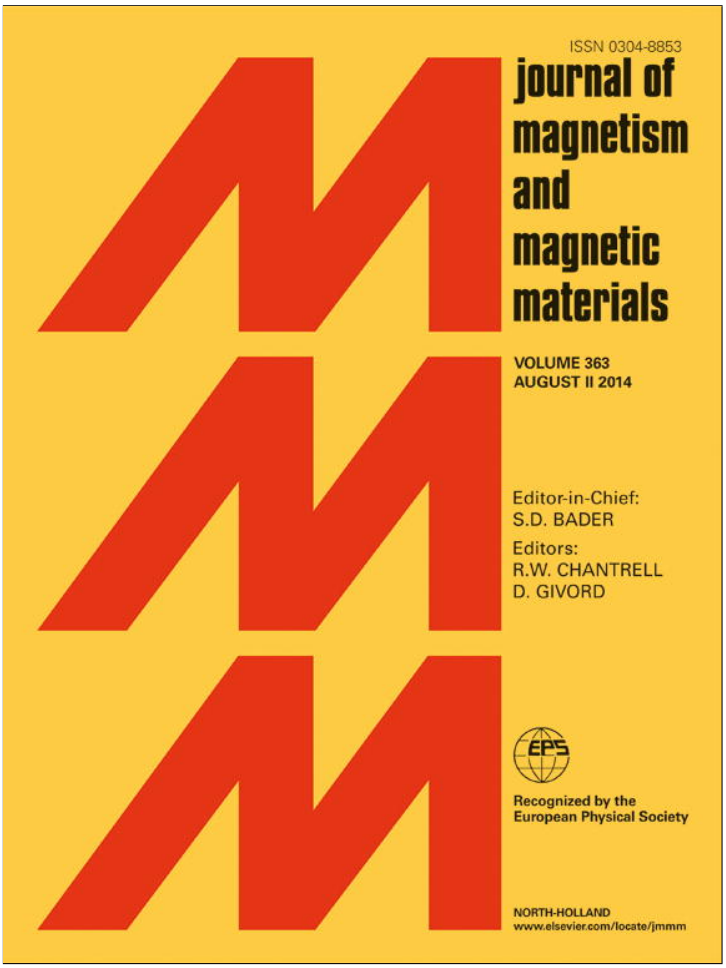

This article appeared in a journal published by Elsevier. The attached copy is furnished to the author for internal non-commercial research and education use, including for instruction at the authors institution and sharing with colleagues.

Other uses, including reproduction and distribution, or selling or licensing copies, or posting to personal, institutional or third party websites are prohibited.

In most cases authors are permitted to post their version of the article (e.g. in Word or Tex form) to their personal website or institutional repository. Authors requiring further information regarding Elsevier's archiving and manuscript policies are encouraged to visit:

http://www.elsevier.com/authorsrights

Author's personal copy

Journal of Magnetism and Magnetic Materials 363 (2014) 82–87

Contents lists available at ScienceDirect

Journal of Magnetism and Magnetic Materials

journal homepage: www.elsevier.com/locate/jmmm

An X- and Q-band Fe^{3+} EPR study of nanoparticles of magnetic semiconductor $Zn_{1-x}Fe_xO$

Sushil K. Misra [a,*], S.I. Andronenko [b], A. Thurber [c], A. Punnoose [c], A. Nalepa [d]

[a] Physics Department, Concordia University, Montreal, QC, Canada H3G 1M8
[b] Physics Institute, Kazan Federal University, Kazan 420008, Russian Federation
[c] Department of Physics, Boise State University, Boise, ID 83725-1570, USA
[d] Max-Planck-Institut für Chemische Energie Konversion, Stifstrasse 34-36, 45470 Mülheim an der Ruhr, Germany

ARTICLE INFO

Article history:
Received 12 March 2013
Received in revised form
25 February 2014
Available online 25 March 2014

Keywords:
EPR
Nanoparticle
ZnO
Dilute magnetic semiconductor
X-band
Q-band
Fe^{3+} ion

ABSTRACT

EPR studies on two types of nanoparticles of Fe^{3+} doped, 0.1–10%, ZnO, NL and QJ, prepared using similar chemical hydrolysis methods, in diethylene glycol, and in denatured ethanol solutions, respectively, were carried out at X-band (~9.5 GHz) at 77 K and at Q-band (~34.0 GHz) at 10, 80, and 295 K. To interpret the experimental results, EPR spectra were simulated by exact diagonalization of the spin-Hamiltonian matrix to identify the Fe ions at different magnetically active sites in these samples. The simulation for NL samples revealed that they contained (i) Fe^{3+} ions, which substituted for Zn ions, the zero-field splitting (ZFS) parameter which has a large distribution over the sample due to oxygen vacancies in the second coordination sphere; (ii) EPR signal from surface oxygen defects; and (iii) ferromagnetically (FM) coupled Fe ions with concentration of Fe more than 1%. The EPR spectra for QJ samples are very different from those for NL samples, exhibiting only rather intense FM EPR lines. The FM and EPR spectra in NL and/or QJ samples are found to vary strongly with differences in the surface morphology of nanoparticles.

© 2014 Elsevier B.V. All rights reserved.

1. Introduction

Dilute magnetic semiconductors (DMSs), containing a small percentage of transition-metal (TM) cations, lead to many new functionalities, resulting from the carrier–cation magnetic exchange. Oxide semiconductors, such as ZnO, have been recently shown to be amongst the most promising host systems to exhibit ferromagnetism (FM) above room temperature [1,2]. Fe^{3+} is among the most appropriate TM ions to exhibit strong FM due to its high magnetic moment of $\sim 5.92\mu_B$ or $\sim 1.73\mu_B$, expected in the high spin ($S=5/2$) or low spin ($S=1/2$) states, respectively.

Fe-doped ZnO nanoparticles are at present considered to be prospective DMS candidates, and have recently been investigated extensively. The various mechanisms for producing ferromagnetism in ZnO nanoparticles are as follows. Dietl et al. [1] first proposed a double-exchange interaction, wherein magnetic ions are coupled by free carriers, resulting in ferromagnetism [3], rendering these materials DMS. A mechanism of bound magnetic polarons (BMPS) has also been proposed to explain magnetic ordering in ZnO [4]. Further investigations revealed that defects could induce ferromagnetic interactions between the dopant Fe ions. On the other hand, antiferromagnetic coupling dominates in neutral defect-free clusters [5]. The ferromagnetic interaction is stabilized in n-type ZnO semiconductors by electron doping [6]. Detailed theoretical studies revealed that the presence of O and Zn vacancies produces ferromagnetism. Ultimately, it was shown that in order to achieve long-range half-metallic ferromagnetism, Zn-vacancies are more crucial than O-vacancies [7]. Finally, the nature of ferromagnetism in DMS is not uniquely established yet. A review of recent advances in the interpretation of ferromagnetism in ZnO was published by Snure et al. [8].

Ferromagnetic interactions exist in these samples near the surface region (within 10 nm) that possess higher Fe concentration, enriched with Zn and O vacancies [9]. Fe^{3+} ions dominate on the surface region, with the ferromagnetism originating from the exchange interaction between an unequal numbers of Fe ions occupying two sets of inequivalent positions in the surface region of 2–3 nm [10]. Karmakar et al. [11] found that the magnetic system of Fe ions becomes converted from the ferromagnetic state to the spin-glass state at $T > 450$ K due to canting of disordered surface-spins in the nanoparticles. The Fe^{3+} ($S=5/2$, $3d^5$) state becomes stabilized in these samples, because XPS studies showed the presence of only Fe^{3+} ions and did not show any significant presence of Fe^{2+} ions [12]. Thus, most of the doped Fe ions are incorporated as Fe^{3+}. As-grown ZnO nanoparticles are n-type semiconductors due to their native defects, which are specifically O- and Zn-vacancies. However, this O-vacancy is too deep in a donor and, therefore, the carriers are not easily excited from donor levels to the conduction band, and a Zn-vacancy is too mobile to be stable, and thus it is not a stable source of carriers.

* Corresponding author.
E-mail address: skmisra@alcor.concordia.ca (S.K. Misra).

http://dx.doi.org/10.1016/j.jmmm.2014.03.031
0304-8853/© 2014 Elsevier B.V. All rights reserved.

Author's personal copy

Therefore, additional doping with Group III ions (B, Al, Ga and In) is required to enhance n-type conductivity in ZnO samples [13]. DMSs are usually formed in $Zn_{1-x}Fe_xO$ nanoparticles at a low concentration (x) of Fe ions, from 0.01% to 0.09%. The disappearance of ferromagnetism at higher concentrations means that Fe ions become incorporated in the secondary magnetic phase, $ZnFe_2O_4$, which is antiferromagnetic at $T_N < 10$ K and paramagnetic at room temperature [14,15]. Alternatively, it can also be ascribed to a transition to the antiferromagnetic state of the $Zn_{1-x}Fe_xO$ phase [16]. On the other hand, if ferrimagnetic Fe_3O_4 ($T_c < 858$ K) is formed as the secondary phase, the magnetic moment increases.

One of the main problems in the study of DMS is the ability to separate the true DMS phase and to avoid the formation of secondary magnetic phases, taking into account the solid-solubility limit of the magnetic dopant. X-ray diffraction (XRD) is not an unequivocal method for the determination of secondary phases in nano-sized particles due to the limited length of Bragg's diffraction. Because of their different crystallographic orientations with respect to the host crystal, secondary-phase nano-particles are very difficult to detect by a simple Bragg–Brentano scan in some cases [3]. With increasing Fe doping, the lattice parameters a and c, and lattice volume V, were determined using suitable pairs of (100), (102), (110) and (103) peaks (and using peak deconvolution as necessary). Usually, several secondary phases were revealed in the $Zn_{1-x}Fe_xO$ system depending on the synthesis method and initial chemical reagents, such as $ZnFe_2O_4$ [15,17], α-Fe [18,19] and Fe_3O_4 [4]. α-Fe and Fe_3O_4 are ferromagnetic and ferrimagnetic, respectively, at room temperature and can mask the true DMS behavior. Therefore, control of secondary magnetic phases is very important in the investigation of DMS. Electron Paramagnetic Resonance (EPR) is a very effective technique in such cases, because it is capable of unambiguously separating the contributions from different sources of magnetism, even for the smallest nanoparticles.

The EPR technique can be used in the investigation of localized Fe impurity ions [10,20,21], localized defects [22–25], and ferromagnetic phases [26] in ZnO nanoparticles. It is a powerful tool to detect secondary magnetic phase formation. The influence on EPR linewidth by charge carriers in semiconducting ZnO [27] provides important information on the mechanism of producing a DMS state. Influence of nanoparticle size and surface defects on magnetic properties of ZnO nanoparticles has been investigated by EPR [28]. Weak exchange interactions of Co^{2+} pairs have also been investigated in ZnO [29]. Controlled formation of defects is a very important step to render Fe-doped ZnO a ferromagnetic semiconductor (DMS) at room temperature, which can be exploited to develop spintronic devices, whose operation depends on both spin and charge of the constituents. Furthermore, several new devices, such as spin transistors and spin-LEDs, have very high-density non-volatile semiconductor memory and optical emitters with polarized output can be fabricated using spintronic materials.

Many EPR investigations of nanoparticles have been reported recently [30–47]. The purpose of this paper is to report detailed EPR studies at X-band (~9.5 GHz) at 77 K and at Q-band (~34 GHz) at 10, 80, and 295 K on two types of nanoparticles of ZnO, NL and QJ, prepared using similar chemical hydrolysis methods, in diethylene glycol, and in denatured ethanol solutions, respectively, doped with 0.1–10% Fe^{3+} to advance further the information available on nanoparticles from EPR.

2. Experimental details

2.1. Synthesis

Special attention is required to synthesize ZnO nanoparticles with controllable surface morphology and size, as the room-temperature ferromagnetism in the $Zn_{1-x}Fe_xO$ system is not stable due to poor reproducibility of defects on the surfaces of ZnO nanoparticles. Two main procedures to grow ZnO nanoparticles have been developed: solid state reactions and solvothermal method [48]. For the latter, two solvents have been used, ethanol [49,50] and diethylene glycol [50], to modify the surfaces of ZnO nanoparticles. Use of diethylene glycol as a solvent produces ellipsoidal (rod-like) samples [51], whereas use of ethanol produces spherical particles [52]. The influence of benzyl alcohol as a solvent on magnetic properties of ZnO was investigated in detail by Clavel et al. [53]. They found that different solvents and capping agents can change the ZnO state from ferromagnetic to paramagnetic. On the other hand, total absence of ferromagnetism in the $Zn_{1-x}Fe_xO$ system for any Fe concentrations was also found [54], whereas the presence of ferromagnetism in pure Wurtzite ZnO phase [20] has also been reported. Thus, the exact mechanism of ferromagnetism in the $Zn_{1-x}Fe_xO$ system is not well understood so far. It is noted in this context that methods of modification of the surface properties and surface charge, strongly influencing the saturation magnetization of ZnO nanoparticles, have been proposed recently [55,56].

Nanoparticle samples of Fe-doped ZnO were synthesized using the chemical hydrolysis of zinc(II) and iron(II) acetate precursors. Two sets of iron-doped zinc oxide nano-samples were prepared using similar chemical hydrolysis methods, one in diethylene glycol, and another in denatured ethanol solutions, hereafter referred to as NL and QJ samples, respectively. The samples were prepared from the same zinc and iron acetate dihydrate precursors. The nano-samples so prepared possess different surface structure/groups depending on the solvent used for synthesis. The dopant concentration, referred to hereafter as x, is given by the molar ratio of [Fe]/([Fe]+[Zn]).

2.2. X-ray diffraction (XRD) characterization and transmission electron microscopy (TEM) images

X-ray diffraction was employed to investigate the structural properties and crystallite size, as well as to rule out the presence of undesired impurity phases. The XRD patterns (Fig. 1) show only the Wurtzite ZnO phase with no indication of the presence of other phases even with up to 10% Fe doping. The XRD peak positions showed gradual changes with Fe doping, revealing significant variations in the unit cell volume, V, which initially increased due to Fe doping by up to 5%. This can be understood qualitatively by realizing the fact that interstitial incorporation of Fe ions results in an expansion of the lattice. This, in turn, causes a rearrangement of neighboring oxygen and/or Zn^{2+} ions for charge neutrality. The relatively mild changes in V for Fe doping > 5% may indicate additional incorporation of dopant ions in both substitutional and interstitial sites, as reported in some host systems, since the Fe^{3+} ionic radius is smaller than that of Zn^{2+}, causing somewhat similar structural changes in the lattice parameters [57]. The average primary crystallite length, L, of the doped $Zn_{1-x}Fe_xO$ nano-samples was calculated using the width of the (102) peak and the Scherrer relation giving $L = 6.8 \pm 1.5$ nm. It was found to be similar for both NL and QJ samples. The sizes of nanoparticles were determined directly by transmission electron microscopy (TEM). Details of size distribution of these nanoparticles were reported by Johnson et al. [12], showing the TEM images of ZnO nanoparticles doped with Fe ions. Studies of such samples by Johnson et al. [12] and by Thurber et al. [58] clearly showed that these samples were nano-sized. As well, they established the intrinsic nature of ferromagnetism in ZnO powder in these samples.

2.3. Saturation magnetization

As seen from the dependence of the saturation magnetization on Fe concentration [58], the saturation magnetization for NL sample with $x = 10\%$ Fe is almost equal to the saturation magnetization for QJ sample with $x = 2.5\%$ Fe. Only when $s > 2.5\%$ Fe does

Author's personal copy

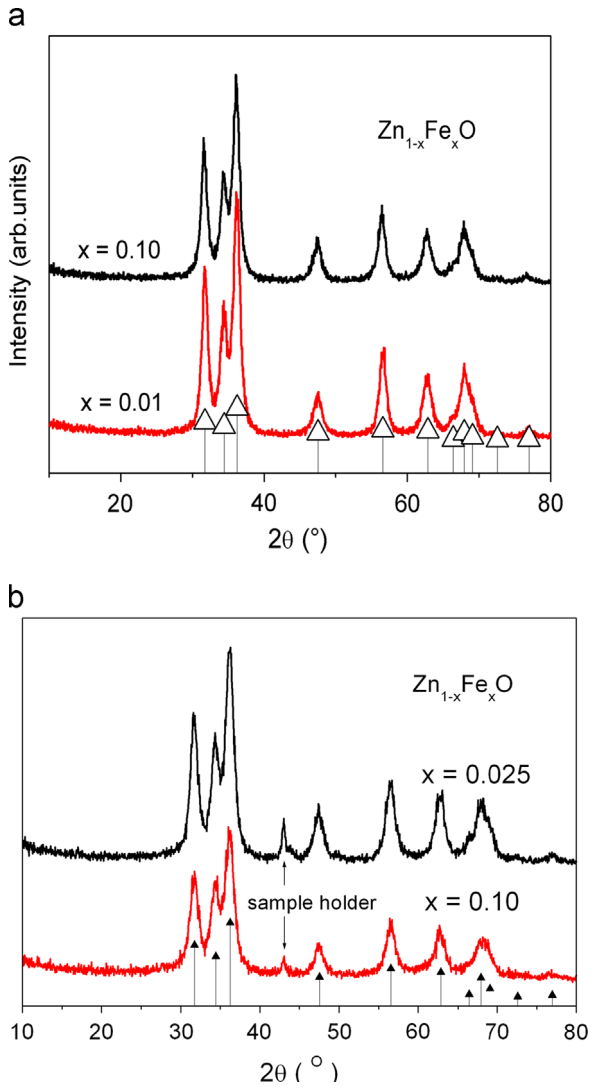

Fig. 1. X-ray diffraction patterns of ZnO nanoparticles doped with Fe ions. (a) NL samples and (b) QJ samples.

the magnetization increase rapidly in QJ samples; this increase does not correlate with the dependence of the unit cell volume on Fe concentration.

3. EPR spectra

X-band spectra were recorded using a conventional X-band Bruker Elexsys E580 spectrometer, operating at 9.505 GHz at Boise State University, and Q-band spectra were recorded by the homemade Q-band spectrometer operating at 34.033 GHz, at Max-Planck Institute for Chemical Energy Conversion, Muelheim an-der-Ruhr, Germany. EPR study of Fe^{3+} ions in $Zn_{1-x}Fe_xO$ NL nanoparticles for $x=0.1\%$, 1%, 2.5%, 7.5%, and 10% was carried out at 77 K to determine the oxidation states of the Fe^{3+} ions, their local environment, interactions, and to find the reasons for the low magnetic moment observed in the magnetization studies. In the present EPR investigation, the same ZnO nanoparticles doped with Fe, as those studied by Johnson et al. [12], were used. The two different kinds of Fe-doped ZnO nanoparticles, NL and QJ, wherein the Fe ions are located on the surfaces, exhibited different EPR spectra. This conclusion has been supported by independent studies [9,10]. The NL spectra reveal three sources of EPR signals: (i) Fe ions, substituting for Zn ions, with oxygen vacancies in their vicinity; (ii) Fe ions in a fully disordered environment; and (iii) uncoupled surface oxygen defects, producing a strong signal at $g=2.003$ [28,41]. In NL samples the EPR spectrum due to localized Fe^{3+} ions disappeared for Fe concentration $x>2.5\%$. On the other hand, QJ samples display only a broad FMR signal, indicative of ferromagnetism, which is much stronger than that in NL samples, because here all Fe ions are ferromagnetically coupled with each other. This intrinsic ferromagnetism of Fe ions is caused by interaction via magnetic F-color centers, i.e. oxygen vacancies, that trap electrons [59]. The difference in the magnetic behaviors of NL and QJ samples is due to the difference in their magnetic interactions, as explained above. The details of EPR spectra at X- and Q-bands are described as follows.

3.1. X-band

The observed EPR spectra at 77 K for both NL and QJ samples are shown in Fig. 2 for samples with different Fe concentrations. *NL samples*. Several groups of EPR lines were observed in the samples with $x=0.1\%$ Fe at 77 K. One of these is due to the Fe^{3+} ions substituting at the Zn sites [30]. The second set of EPR lines is characterized by linewidths from 3 to 10 mT, located at 340, 280, and 180 mT, which can be ascribed, respectively, to the transitions $-1/2\leftrightarrow+1/2$ (allowed), $-3/2\leftrightarrow3/2$ (forbidden), and $-5/2\leftrightarrow5/2$ (forbidden). In addition, a transition at $\sim$300 mT is also observed, which can be ascribed to some iron clusters with $S>5/2$. The third is the EPR line with $g=2.003$, which belongs probably to the well-known surface oxygen defects [28,41]. In addition, another set of EPR lines was observed, which broadened with increasing Fe concentration, so that only one broad paramagnetic line of width about 45 mT, along with a ferromagnetic line with $g=2.1$ and linewidth 125 mT, was observed for the Fe concentrations $x\geq2.5\%$. Similar EPR lines were observed by Karmakar et al. [11]. The proportion of the very broad FM line changes with concentration, with the maximum value being observed for $x=10\%$ Fe. It is noted that the EPR spectra for the undoped ZnO nanoparticles prepared using the NL method displayed a very weak EPR signal, which is similar, but much weaker than what is seen in the 0.1% Fe doped sample. This signal is most likely due to unintentional incorporation of a minute fraction of transition metal ions, most likely Fe ions. A weak EPR signal due to Mn^{2+} ion is clearly seen in this sample (Fig. 3).*QJ samples*. Only broad ferromagnetic EPR signals were observed in these samples, which are much stronger than those observed in NL samples. They are characterized by $g=2.00\pm$

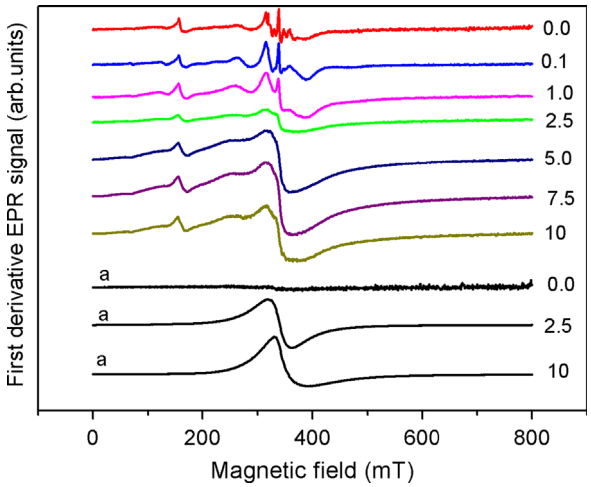

Fig. 2. X-band Fe^{3+} EPR spectra of ZnO nanoparticles in NL and QJ samples doped with different concentrations of Fe ions. The EPR spectra of QJ samples are indicated by **a**. The intensities of EPR spectra for different Fe concentrations are in arbitrary units.

Author's personal copy

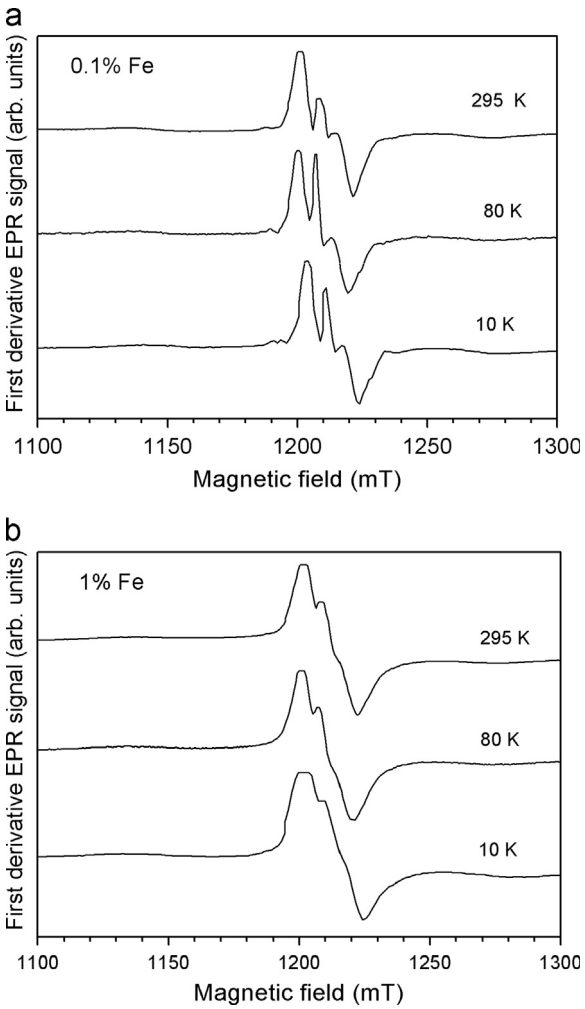

Fig. 3. Q-band (~34.0 GHz) Fe^{3+} EPR spectra of nanoparticle of ZnO doped with 0.1% (a) and 1% (b) Fe (NL sample) at 10, 80 and 295 K.

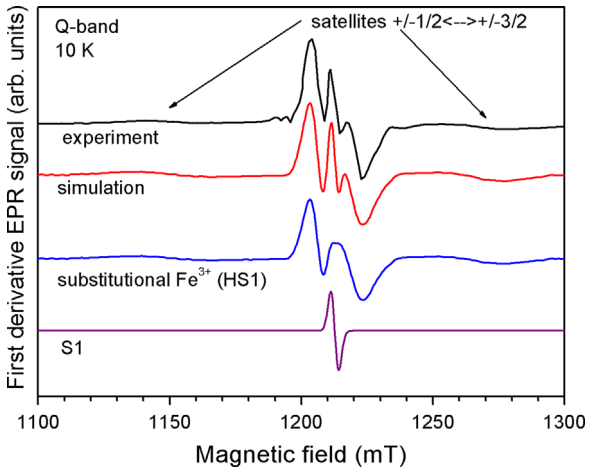

Fig. 4. Q-band experimental and simulated Fe^{3+} EPR spectra (NL samples) at 10 K in a nanoparticle of ZnO, doped with 0.1% Fe. The simulated spectrum is the sum of HS1 and S1 spectra.

0.02, with the linewidth of 45 mT for the sample with $x=2.5\%$ Fe, and by $g=1.89\pm0.02$ with the linewidth of 58.7 mT for the sample with $x=10\%$ Fe. The latter signal is not symmetric, indicating that it is overlapped by another smaller signal. No presence of isolated Fe^{3+} ions was exhibited by the EPR spectra of QJ samples, showing that all the Fe ions in QJ samples are coupled by exchange interactions, probably via the O- and Zn-defects. The undoped QJ samples seem to be pure with no sign of unintentional dopants unlike that for the undoped NL sample, as confirmed by their EPR spectra.

3.2. Q-band spectra of NL samples

3.2.1. Experimental

The Q-band (~34 GHz) EPR spectra of Fe^{3+} ions in $Zn_{1-x}Fe_xO$ nanoparticles in NL samples for $x=0.1$ and 1, shown in Figs. 3a and 3b, provided more details than those at X-band, enabling a more accurate determination of the spin-Hamiltonian (SH) parameters. At least two groups of EPR lines were observed, similar to those at X-band. One of these is due to the Fe^{3+} ions substituting at Zn sites, with trigonal point-group symmetry [30,31]. The second one is due to the oxygen defects on the nanoparticle surface [28,41]. The first EPR spectrum is similar to the more intense trigonal Fe^{3+} spectrum in bulk ZnO [30], but associated with large distribution of the ZFS (B_2^0) parameter due to the vacancies in the second coordination sphere. There were also observed low- intensity signals with $g\sim4.0$, $g\sim6.0$ and $g\sim10.0$, similar to those observed at X-band. However, the relative intensities of these low field lines at Q-band are much less than those observed at X-band. This is because they are forbidden transitions, whose intensities decrease with increasing microwave frequency. These Q-band EPR spectra do not change significantly with temperature. The EPR linewidth for the sample with 1% Fe is larger than that for the sample with 0.1% Fe due to the increased dipole–dipole interactions between the Fe ions. The Q-band Fe^{3+} spectrum in the samples with concentrations of 0.1% and 1% Fe are shown in Figs. 3a and b, respectively. With increasing concentration of Fe ions the EPR lines broaden, resulting in the disappearance of the outer $\pm1/2 \leftrightarrow \pm3/2$ and $\pm3/2 \leftrightarrow \pm5/2$ transitions.

3.2.2. Simulation of Fe^{3+} EPR spectra for NL samples

The experimental and simulated Fe^{3+} EPR spectra at Q-band at 10 K in the NL sample with Fe concentration of 0.1% are shown in Fig. 4. The simulated spectrum consists of an overlap of the simulated spectra HS1 and S1, whose interpretations are given below. Only Q-band spectra were simulated here, because the B_2^0 parameter for the trigonal site of Fe^{3+} in ZnO is rather large, which makes the simulation easier.

The allowed Fe^{3+} fine-structure transitions ($\Delta M=\pm1$ where M is the electronic magnetic quantum number) line positions in the samples were simulated well by using the axial spin-Hamiltonian (SH) [60]:

$$H=\mu_B g B\, S+B_2^0 O_2^0 \quad (1)$$

Here, μ_B is the Bohr magneton; S ($=5/2$) is the electronic spin of the Fe^{3+} ion; $\boldsymbol{B}$ is the external magnetic field; B_2^0 is the zero-field splitting (zfs) parameter; and O_2^0 is the operator equivalent as defined by Abragam and Bleaney [60,61]. In particular, the observed EPR spectrum can be simulated reasonably well, using the SH given by Eq. (1), as an overlap of two spectra, HS1 and S1, due to high-spin ($S=5/2$) Fe^{3+} ions, and oxygen defects ($S=1/2$) on the nanoparticle surface, respectively, as evaluated by trial-and-error simulation with exact diagonalization of the SH matrix. The HS1 spectrum is, in turn, due to an overlap of several Fe^{3+} spectra with the values of the zfs (B_2^0) ranging from –0.13 to $0.30\times10^{-4}\,cm^{-1}$, whose intensities follow a Gaussian distribution, centered at $B_2^0=-193\times10^{-4}\,cm^{-1}$, with the Gaussian width, w, being $0.78\times10^{-4}\,cm^{-1}$, required to simulate the EPR lines, for the $\pm1/2 \leftrightarrow \pm3/2$ transitions. (The transitions $\pm3/2 \leftrightarrow \pm5/2$ were totally broadened out due to the rather large distribution of B_2^0 [60].) The two sets of SH parameters for HS1 and S1 are listed in

Author's personal copy

Table 1
The spin-Hamiltonian parameters for Fe^{3+} ions substituting for Zn ions in ZnO NL sample, doped with 0.1% Fe at Q-band, corresponding to the HS1 spectrum, for which the spin $S=5/2$. Here B_2^0 is the zfs parameter, and w is the parameter of Gaussian distribution of B_2^0. The S1 spectrum is due to the oxygen defects ($S=1/2$) present on the nanoparticle surface. ΔB is equal to one-half of the peak-to-peak first-derivative EPR line width.

$Zn_{1-x}Fe_xO$ ($x=0.1$)	Spectrum	g	B_2^0 (10^{-4} cm^{-1})	w (10^{-4} cm^{-1})	ΔB (10^{-4} cm^{-1})
$S=5/2$	HS1	2.006	−193	78	19
$S=1/2$	S1	2.003	0	–	14

Table 1. The sign of B_2^0 has been reported to be negative [31], which was then used here and reported in Table 1.

3.2.2.1. Interpretation of HS1 spectrum. The HS1 EPR spectrum is due to those Fe^{3+} ions, which substitute for Zn ions in ZnO in the crystal lattice. This spectrum is similar to that observed in bulk ZnO single crystal [30]. Increase in the number of oxygen vacancies in ZnO nanoparticles occurs as a consequence of the increased total surface area of nanoparticles. The HS1 spectrum is due to mainly Fe^{3+} sites in the "core" area of nanoparticles. When the size of ZnO nanoparticles is much less (~7 nm), the surface area, enriched with oxygen defects, increases, and more defects appear in the close vicinity of the impurity Fe ions, leading to a distribution of local crystal fields at the Fe sites. This results in a distribution of B_2^0 SH parameter. The parameter of Gaussian distribution, w, of B_2^0 around its average value is then a measure of the distribution of the defects in ZnO nanoparticles in the volume between the surface area, where there exists the maximum concentration of defects, and the core area, where there exists the regular crystal lattice without defects.

3.2.2. Interpretation of S1 spectrum

The EPR spectrum with a rather intense central line at $g=2.003$ and linewidth 2.3 mT, is due to surface oxygen defects, well known in ZnO nanoparticles [30,41]. This line exists only in NL samples at both X- and Q-bands; it does not appear in QJ samples.

4. Discussion

There are two aspects of EPR spectra, which are worthy of discussion, as discussed below.

4.1. Coexistence of ferromagnetic and paramagnetic states in NL samples in ZnO

As discussed below, ferromagnetism occurs in the regions, which are rich in oxygen vacancies. On the other hand, there exist some regions, wherein Fe ions are not bound together through exchange interactions due to lack of oxygen vacancies. These localized Fe ions provide a paramagnetic signal. Consequently, both paramagnetic and ferromagnetic EPR signals coexist in ZnO nanoparticles.

4.2. Occurrence of ferromagnetism

Ferromagnetic order occurs due to oxygen vacancies in the samples with Fe dopant concentration $x \geq 2.5\%$, as seen in the X-band spectra in NL samples, for which the paramagnetic EPR Fe spectrum co-exists with the large FM signal. There have been several mechanisms proposed for these. (i) FCE (F-center exchange) model of ferromagnetism, as proposed by Coey et al. [59]. Here ferromagnetic coupling of ferric ions occurs via an electron trapped in a bridging oxygen vacancy (F center). They explain that $Fe^{3+}-\square-Fe^{3+}$ groups, where $\square$ denotes an oxygen vacancy, are common in the structure and can be considered as a magnetic polaron. An electron that gets trapped in the oxygen vacancy constitutes, what is known as an F-center, where the electron occupies an orbital that overlaps the d-shells of both the iron neighbors. The radius of the electron orbital is of the order $a_o\varepsilon$, where a_o is the Bohr radius and ε is the dielectric constant of the sample. Since Fe^{3+} ($3d^5$) has only minority spin orbitals unoccupied, the trapped electron is oriented with its spin down (↓), and the two iron neighbors will have their spins pointing up (↑). In the regions with increased density of oxygen vacancies, ferromagnetically coupled networks exist, containing Fe^{3+}–□–Fe^{3+} groups, which exhibit ferromagnetic EPR signals. (ii) Recently, Coey et al. [62] suggested another mechanism, based on charge transfer in defected oxides. They invoked the model of Stoner, in which the ferromagnetism arises due to the defect-band electron structure of semiconducting ZnO. Furthermore, as seen from Fig. 2, there appear no EPR lines due to localized Fe^{3+} ions in QJ samples, implying that all the Fe ions are coupled ferromagnetically in these samples.

5. Concluding remarks

The salient features of the present X- and Q-band EPR study on two different types of nanoparticles, NL and QJ, of Fe-doped ZnO are as follows.

(i) The observed EPR spectra in NL samples with Fe concentration of more than 2.5% provide clear evidence for the coexistence of isolated paramagnetic Fe^{3+} ions exhibiting sharp EPR lines, and ferromagnetically coupled Fe ions producing a single broad ferromagnetic resonance line.
(ii) The spin-Hamiltonian parameters for HS1 and S1 spectra exhibited by NL samples have been estimated. The HS1 EPR line for isolated Fe^{3+} ions has been successfully simulated here by taking into account a Gaussian distribution of the zfs (B_2^0) parameter.
(iii) The paramagnetic fraction of the doped ions in NL samples does not contribute to the magnetization of the samples, as they are not exchange-coupled, explaining the smaller magnetization observed in NL samples.
All the doped Fe ions in QJ samples are magnetically coupled via oxygen defects. Thus, they only exhibit ferromagnetic resonance signals, which are much stronger than those observed in NL samples. This explains their stronger magnetization as compared to that of NL samples.

Acknowledgments

This research was supported by the Natural Sciences and Engineering Research Council of Canada (NSERC) (SKM), and by the National Science Foundation Grants EAGER DMR-1137419 and CBET 1134468 (AP). SIA is grateful to Ministry of Education of Russian Federation within the framework of the Project RNP-31, for partial support.

References

[1] T. Dietl, H. Ohono, F. Matsukura, J. Cibert, D. Ferrand, Zener model description of ferromagnetism in zinc-blende magnetic semiconductors, Science 287 (2000) 1019–1022.
[2] K. Sato, H. Katayama-Yoshida, Electronic structure and ferromagnetism of transition metal-impurity-doped zink oxide, Physica B: Condens. Matter 308–310 (2001) 904–907.

Author's personal copy

[3] Shengqiang Zhou, K. Potzger, Qingyu Xu, G. Talut, M. Lorenz, W. Skorupa, M. Helm, J. Fassbender, M. Grundmann, H. Schmidt, Ferromagnetic transition metal implanted ZnO: a diluted magnetic semiconductor, Vacuum 83 (2008) S13–S19.

[4] X.X. Wei, C. Song, K.W. Geng, F. Zeng, B. He, F. Pan, Local Fe structure and ferromagnetism in Fe-doped ZnO films, J. Phys.: Condens. Matter 18 (2006) 7471–7479.

[5] N. Ganguli, I. Dasgupta, B. Sanyal, The making of ferromagnetic Fe doped ZnO nanoclusters, Appl. Phys. Lett. 94 (2009) 192503.

[6] K. Sato, H. Katayama-Yoshida, Stabilization of Ferromagnetic States by Electron Doping in Fe-, Co- or Ni-Doped ZnO, Jpn. J. Appl. Phys. 40 (2001) L334–L336.

[7] D. Karmakar, I. Dasgupta, G.P. Das, Y. Kawazoe, High temperature ferromagnetism in Fe-doped ZnO: a density functional investigation, Mater. Trans. 48 (2007) 2119–2122.

[8] M. Snure, D. Kumar, A. Tiwari, Minerals, Progress in ZnO-based diluted magnetic semiconductors, Met. Mater. Soc 61 (2009) 72–75.

[9] P. Wu, G. Saraf, Y. Lu, D.H. Hill, D.A. Arena, R.A. Bartynski, F. Cosandey, J.F. Al-Sharab, L. Wielunski, R. Gateau, J. Dvorak, A. Moodenbaugh, J.A. Raley, Yung Kee Yeo, Magnetic properties of Fe-implanted ZnO Nanotips grown by metal-organic chemical vapor deposition, J. Electron. Mater. 36 (2007) 529–532.

[10] T. Kataoka, M. Kobayashi, Y. Sakamoto, G.S. Song, A. Fujimori, F.H. Chang, H. J. Lin, D.J. Huang, C.T. Chen, T. Ohkochi, Y. Takeda, T. Okane, Y. Saitoh, H. Yamagami, A. Tanaka, S.K. Mandal, T.K. Nath, D. Karmakar, I. Dasgupta, Electronic structure and magnetism of the diluted magnetic semiconductor Fe-doped ZnO nanoparticles, J. Appl. Phys. 107 (2010) 033718.

[11] D. Karmakar, S.K. Mandal, R.M. Kadam, P.L. Paulose, A.K. Rajarajan, T.K Nath, A. K. Das, I. Dasgupta, G.P. Das, Ferromagnetism in Fe-doped ZnO nanocrystals: experimental and theoretical investigations, Phys. Rev. B 75 (2007) 144407.

[12] L.M. Jonhson, A. Thurber, J. Anghel, M. Sabetian, M.H. Engelhard, D.A. Tenne, C. B. Hanna, A. Punnoose, Transition metal dopants essential for producing ferromagnetism in metal oxide nanoparticles, Phys. Rev. B 82 (2010) 1054419-1–5054419-5 (054419).

[13] M.D. McCluskey, S.J. Jokela, Defects in ZnO, J. Appl. Phys. 106 (2009) 071101.

[14] Geun Young Ahn, S.J. Seung-Iel Park, S.J. Kim, Bo Wha Lee, Chul Sung, Preparation of Fe-doped ZnO ferromagnetic semiconductor by sol-gel method with hydrogen treatment, IEEE Trans. Magn. 41 (2005) 2730–2732.

[15] Huilian Liu, Jinghai Yang, Yongjun Zhang, Yaxin Wang, Maobin Wei, Ferromagnetism and exchange bias in Fe-doped ZnO nanocrystals, Mater. Chem. Phys. 112 (2008) 1021–1023.

[16] Prashant K. Sharma, Ranu K. Dutta, Avinash C. Pandey, Samar Layek, H. C. Verma, Effect of iron doping concentration on magnetic properties of ZnO nanoparticles, J. Magn. Magn. Mater. 321 (2009) 2587–2591.

[17] J.S. Shim, T. Hwang, S. Lee, J.H. Park, S.-J. Han, Y.H. Jeong, Origin of ferromagnetism in Fe- and Cu- codoped ZnO, Appl. Phys. Lett. 86 (2005) 082503.

[18] Y.R. Uum, B.S. Han, H.M. Lee, S.M. Hong, G.M. Kim, C.K. Rhee, Magnetic and photocatalytic effect of Fe-doped nano-rod ZnO synthesized by the hydrolysis of metal powders, Phys. Stat. Solidi C 4 (2007) 4408–4411.

[19] K. Potzger, Shengqiang Zhou, H. Reuter, A. Mucklich, F. Eichhorn, N. Schell, W. Scorupa, M. Helm, J. Fassbender, T. Herrmannsdorfer, T.P. Papageorgiou,, Fe implanted ferromagnetic ZnO, Appl. Phys. Lett. 88 (2006) 052508.

[20] Xu Zuo, Soack-Dae Yoon, Aria Yang, Wen-Hui Duan, C. Vittoria, V.G Harris, Ferromagnetism in pure wurtzite zinc oxide, J. Appl. Phys. 105 (2009) 07C508.

[21] Z.-Y. Yang, Studies of the EPR parameters and defect structure for tetrahedral Fe^{3+} centers in zinc oxide, Phys. S tatus Solidi B 246 (2009) 1919–1924.

[22] J.-F. Li, X.-Y. Kuang, A.-J. Mao, X.-M. Tan, EPR theoretical study of local molecular structure for tetrahedral Fe^{3+} centers in zinc oxide, Chem. Phys. Lett. 429 (2006) 266–270.

[23] A. Singhal, S.N. Achary, A.K. Tyagi, P.K. Manna, S.M. Yusuf, Colloidal Fe-doped ZnO nanocrystals: facile low temperature synthesis, characterization and properties, Mater. Sci. Eng. B 153 (2008) 47–52.

[24] G. Glaspell, P. Dutta, A. Manivannan, A room-temperature and microwave synthesis of M-doped ZnO (M=Co, Cr, Fe, Mn & Ni), J. Clust. Sci. 16 (2005) 523–536.

[25] N.G. Romanov, D.O. Tolmachev, A.G. Badalyan, R.A. Babunts, P.G. Baranov, V. V. Dyakonov, Spin-dependent recombination of defects in bulk ZnO crystals and ZnO nanoparticles as studied by optically detected magnetic resonance, Physica B: Cond. Matt 404 (2009) 4783–4786.

[26] Y. Zhang, S.-s. Yan, Y.-h. Lui, Y. Tian, G. Liu, Y. Chen, L. Mei, J.P. Liu, Ferromagnetic resonance study on Fe-ZnO inhomogeneous magnetic semiconductors, Solid State Commun. 140 (2006) 405–409.

[27] N.C. Giles, N.Y. Garces, L.E. Lijun Wang, Halliburton, Photoluminescence and EPR of donors and acceptors in ZnO, quantum sensing and nanophotonic devices, Proc. SPIE 5359 (2004) 267–278.

[28] P. Jakes, E. Erdem, Finite size effects in ZnO nanoparticles: an electron paramagnetic resonance (EPR) analysis, Phys. Status Solidi (RRL) 5 (2011) 56–58.

[29] D.V. Azamat, A. Dejneka, V.A. Trepakov, L. Jastrabik, M. Fanciulli, V.Y. Ivanov, M. Godlewski, V.I. Sokolov, J. Rosa, A.G. Badalyan, Photo-EPR and magneto-optical spectroscopy of iron centers in ZnO, Phys. Status. Solidi (RRL) 5 (2011) 138–140.

[30] W.M. Walsh Jr., L.P. Rupp Jr., Paramagnetic resonance of trivalent Fe57 in zinc oxide, Phys. Rev. 126 (1962) 952–955.

[31] D.A. Azamat, M. Fanciulli, The structure of charge-compensated Fe^{3+} ions in ZnO, Physica B: Condens. Matter. 401–402 (2007) 382–385.

[32] T.X. Chen, L. Cao, W.H. Zhang, W. Zhang, Y.Y. Han, Z.Y. Zheng, F.Q. Xu, I Kurash, H.J. Qian, J.O. Wang, Correlation between electronic structure and magnetic properties of Fe-doped ZnO films, J. Appl. Phys. 111 (12) (2012) 123715 (8).

[33] R. Heitz, A. Hoffmann, I. Broser, Fe^{3+} center in ZnO, Phys. Rev. B 45 (16) (1992) 8977–8988.

[34] X.Y. Kuang, Ground-state zero-field splitting of Fe^{3+} ion in ZnO and CdSe crystals, Phys. Status Solidi B 197 (1) (1996) 225–230.

[35] K. Matsuki, J. Kimura, N. Sakagami, H. Satoh, A. Onodera, Electron spin resonance of Fe^{3+} ions in ZnO single crystal, Ferroelectrics 272 (1) (2002) 181–185.

[36] J.F. Piamba, J.C. Paz, L.E. Zamora, G.A.P. Alcazar, Study of Fe-doped ZnO by mechanical alloying, J. Supercond. Novel Magn. 25 (7) (2012) 2223–2226.

[37] J. Tribollet, J. Behrends, K. Lips, Ultra long spin coherence time for Fe^{3+} in ZnO: Aa new spin qubit, Eur. Phys. Lett 84 (2) (2008) 20009.

[38] Yu. S. Kutin, G.V. Mamin, S.B. Orlinskii, Identification of Fe^{3+} - Li- complexes in ZnO by means of high-frequency EPR/ENDOR spectroscopy, J. Mag. Reson. 237 (2013) 110–114.

[39] P. Zhang, T.L. Phan, S.C. Yu, Electron-spin-resonance study of polycrystalline Fe-doped ZnO ceramics, J. Korean Phys. Soc. 61 (10) (2012) 1563–1567.

[40] H. Kaftelen, K. Ocakoglu, S. Tu, R. Thomann, S. Weber, E. Erdem, EPR and photoluminescence studies on the defect structure of ZnO nanocrystals, Phys. Rev. B 86 (2012) 014113.

[41] S.K.S. Parashar, B.S. Murty, S. Repp, S. Weber, E. Erdem, Investigation of intrinsic defects in core-shell structured ZnO nanocrystals, J. Appl. Phys. 111 (2012) 113712.

[42] K. Hoffmann, D. Hahn, Electron-spin resonance of lattice-defects in zinc oxide, Phys. Status Solidi A 24 (2) (1974) 637–648.

[43] S.K. Misra, S.I. Andronenko, A. Punnoose, D. Tipikin, J.H. Freed, A 236-GHz Fe^{3+} EPR study of nano-particles of the ferromagnetic room-temperature semiconductor $Sn_{1-x}Fe_xO_2$ ($x=0.005$), Appl. Magn. Reson. 36 (2009) 291–295.

[44] A. Punnoose, K.M. Reddy, J. Hayes, A. Thurber, S. Andronenko, S.K Misra, Dopant spin states and magnetic interactions in transition metal doped semiconductor particles, Appl. Magn. Reson. 36 (2009) 331–345.

[45] S.K. Misra, S.I. Andronenko, S. Rao, V.B. Bhat, C. Van Komen, A Punnoose, Cr^{3+} electron paramagnetic resonance study of $Sn_{1-x}Cr_xO_2$($0.00\leq x\leq 0.10$), J. Appl. Phys. 105 (2009) 07C514.

[46] S.K. Misra, S.I. Andronenko, K.M. Reddy, J. Hays, A. Thurber, A. Punnoose, A variable temperature Fe^{3+} electron paramagnetic resonance study of $Sn_{1-x}Fe_xO_2$ ($0.00\leq x\leq 0.05$), J. Appl. Phys. 101 (2007) 09H120.

[47] S.K. Misra, S.I. Andronenko, K.M. Reddy, J. Hays, A. Punnoose, Electron Paramagnetic Resonance studies of Co^{2+} ions in nanoparticles of SnO_2 processed at different temperatures, J.Appl. Phys. 99 (2006) (08 M10608M106).

[48] C. Satienpattanakoon, D. Yiamsawas, W. Kangwansupamonkon, R Nuisin, Synthesis and characterization of Zinc Oxide Nanocrystals by solid-state and solvothermal techniques, Adv. Mater. Res. 55–57 (2008) 657–660.

[49] A. Parra-Palomino, O. Perales-Perez, R. Singhal, M. Tomar, J. Hwang, P. M. Voyles, Structural, optical, and magnetic characterization of monodisperse Fe-doped ZnO nanocrystals, J. Appl. Phys. 103 (2008) 07D121.

[50] Ch.-H. Hsien, Spherical zinc oxide nano particles from zinc acetate in precipitation method, J. Chin. Chem. Soc. 54 (1) (2007) 31–34.

[51] Y. Hu, H.J. Chen, Preparation and characterization of nanocrystalline ZnO particles from a hydrothermal process, J. Nanopart. Res. 10 (3) (2008) 401–407.

[52] J. Alaria, M. Venkatesan, J.M.D. Coey, Magnetism of ZnO nanoparticles doped with 3d cations prepared by a solvothermal method, J. Appl. Phys. 103 (2008) 07D123.

[53] G. Clavel, M.-G. Willinger, D. Zitoun, N. Pinna, Solvent Dependent shape and magnetic properties of doped ZnO nanostructures, Adv. Funct. Mater. 17 (2007) 3159–3169.

[54] Z.H. Zhang, Xuefeng Wang, J.B. Xu, S. Muller, C. Ronning, Quan Li, Evidence of intrinsic ferromagnetism in individual dilute magnetic semiconducting nanostructures, Nat. Nanotechnol. 4 (2009) 523–527.

[55] A. Thurber, G.A. Alanko, G.L. Beausoleil II, K. Dodge, Ch. Hanna, A. Punnoose, Unusual crystallite growth and modification of ferromagnetism due to aging in pure and doped ZnO nanoparticles, J. Appl. Phys. 111 (2012) 07C319.

[56] J. Zhang, G. Dong, A. Thurber, Y. Hou, M. Gu, D.A. Tenne, C.B. Hanna, A Punnoose, Tuning the properties of ZnO hematite and Ag nanoparticles by adjusting the surface charge, Adv. Mater. 24 (2012) 1232–1237.

[57] J. Hays, A. Punnoose, R. Baldner, M.H. Engelhard, J. Peloquin, K.M Reddy, Relation between the structural and magnetic properties of Co-doped SnO_2 nanoparticles, Phys. Rev. B 72 (2005) 075203.

[58] A. Thurber, G. Beausoleil, G. Alanko, J. Angel, M. Jones, L. Johnson, J Zhang, C. Hanna, D. Tenne, A. Punnose, Magnetism of ZnO nanoparticles: dependence on crystalline size and surfactant coating, J. Appl. Phys. 109 (2011) 07C305 (3).

[59] J.M.D. Coey, A.P. Douvalls, C.B. Fitzgerald, M. Venkatesan, Ferromagnetism in Fe-doped SnO_2 thin films, Appl. Phys. Lett. 84 (2004) 13332.

[60] A. Abragam, B. Bleaney, Electron Paramagnetic Resonance of Transition Ions, Clarendon Press, Oxford, 1970.

[61] S.K. Misra, in: S.K. Misra (Ed.), Multifrequency Electron Paramagnetic Resonance: Theory and Applications, Wiley-VCH, Weinheim, Germany, 2011.

[62] J.M.D. Coey, P. Stamenov, P.D. Gunning, M. Venkatesan, K. Paul, Ferromagnetism in defect-ridden oxides and related materials, New J. Phys. 12 (2010) 053025.